Quantitative vibrational sum-frequency generation spectroscopy of thin layer electrochemistry: CO on a Pt electrode

ARTICLE *in* SURFACE SCIENCE · JULY 2005

Impact Factor: 1.93 · DOI: 10.1016/j.susc.2005.02.041

4 AUTHORS, INCLUDING:

Alexei Lagutchev
Purdue University
44 PUBLICATIONS **720** CITATIONS
SEE PROFILE

Dana D Dlott
University of Illinois, Urbana-Champaign
297 PUBLICATIONS **6,640** CITATIONS
SEE PROFILE

Available online at www.sciencedirect.com
SCIENCE DIRECT®
Surface Science 585 (2005) 3–16
SURFACE SCIENCE
www.elsevier.com/locate/susc

Quantitative vibrational sum-frequency generation spectroscopy of thin layer electrochemistry: CO on a Pt electrode

G.Q. Lu, A. Lagutchev, Dana D. Dlott, A. Wieckowski *

Frederick Seitz Materials Research Laboratory and School of Chemical Sciences, University of Illinois at Urbana-Champaign, 600 S. Mathews Avenue, Urbana, IL 61801, USA

Available online 19 April 2005

Abstract

Simultaneous electrochemical and vibrational sum-frequency generation (SFG) spectroscopy measurements are made of oxidation of CO on a polycrystalline Pt electrode with both CO-free and CO-saturated electrolytes. A femtosecond broad-band multiplex SFG apparatus permits rapid spectral acquisitions (5 s^{-1}) synchronized with the potential sweep at a rate of 5 mV/s. The electrochemical cell has an ideal configuration, where the thickness of the supporting electrolyte (here 25 μm) was controlled by a spacer. The SFG lineshape is analyzed with a method that extracts the amplitude, peak frequency and Lorentzian linewidth of the CO stretch resonance as well as the nonresonant contribution from the Pt electrode. With a CO-free electrolyte, it is shown that the loss of SFG signal from CO quantitatively tracks the CO surface coverage, as determined by the integrated current or charge. The CO peak shift undergoes Stark tuning at a rate of 27.5 ± 1 cm^{-1} V^{-1} until an electrode potential slightly below the onset of CO oxidation. As CO is oxidized, the peak frequency dips and then recovers, while the peak linewidth broadens and then narrows. These effects are more pronounced with CO-saturated electrolyte. The relationships between the CO peak shift and linewidth and the microscopic dynamics of CO at the electrochemical surface are discussed briefly.

Keywords: Sum-frequency generation; SFG; Broadband; Dynamics; Thin layer electrochemistry; Platinum; CO chemisorption; Voltammetry

1. Introduction

Vibrational sum-frequency generation spectroscopy (SFG) has emerged as a promising technique to probe the in situ dynamics of molecules adsorbed at electrode surfaces [1–4]. CO electrochemistry at a

* Corresponding author. Tel.: +1 217 333 7943; fax: +1 217 244 8068.
E-mail address: andrzej@scs.uiuc.edu (A. Wieckowski).

0039-6028/$ - see front matter © 2005 Published by Elsevier B.V.
doi:10.1016/j.susc.2005.02.041

platinum electrode has of course been intensively studied [5–17], and has become a model surface reaction in electrochemistry [1,4,18–21]. In previous works, the loss of SFG signal from electrosorbed CO on Pt has been associated with the loss of CO coverage resulting from CO oxidation. However the detailed nature of this association and the relationships between SFG spectra and adsorbate molecular dynamics have not yet been examined carefully.

Baldelli et al. [2], using a CO-free 0.5 M H_2SO_4 electrolyte, reported that the CO SFG signal disappeared almost 200 mV below the CO oxidation threshold, which was interpreted as resulting from the electrochemical generation of an SFG-invisible CO adsorption state. Since the electric field component of the SFG probe vanishes at a metallic surface, this proposed invisible CO state was suggested to involve CO parallel to the Pt surface. Dederichs et al. [3] also reported CO signal disappearance prior to the oxidation threshold using a CO-saturated 0.1 M $HClO_4$ electrolyte, which was attributed to CO depletion in the quite thin electrolyte layer. Recent measurements by Chou et al. [4] were interpreted to show that the CO stretch peak vanished immediately after the oxidation current reached its maximum. The SFG signal also showed a substantial increase (nearly doubling) in the run up to oxidation threshold.

Although it seems reasonable to expect SFG signal disappearance during electrooxidation to correspond to loss of CO coverage, there are a number of reasons why this correspondence need not be precise, and a number of reasons why experimental determination of the extent of correspondence has so far proven elusive. The most obvious reason is that the electrochemistry might not be done properly. For instance the assignment of a CO-invisible state by Baldelli et al. [2] is now believed to be incorrect [4], resulting from the comparison of an accurate measurement of stripping potential obtained in less than one minute with problematic electrochemistry measured during SFG runs occurring over the 20–60 min time scale. Clearly the need for slow scan rates to obtain SFG spectra in these cited works greatly increased the possibilities for contamination and problematic electrochemical oxidation.

As with all spectroscopic techniques, the SFG signal intensity depends on both molecular number density (coverage) and transition strength (cross-section), and for a coherent nonlinear technique this dependence can be more complicated [22] than with more usual linear techniques such as infrared absorption spectroscopy (IRAS) [9,23]. The usual way to interpret IRAS measurements in electrochemistry is to subtract off the background and measure the area of the CO vibrational peak [9,23]. It is better to measure the area than the peak height because the width might be changing during the electrochemistry. In SFG, one ordinarily expects the integrated area of the resonant transition to be proportional to the square of the number density [22]. But in an electrochemical cell there is an additional complication. The SFG signal is a coherent admixture of the resonant CO vibrational transition and a broader nonresonant background from the metallic surface [24,25]. Depending on the relative magnitudes of the two contributions, the CO signal intensity could be proportional to the surface coverage raised to any power between one and two. Thus the SFG signal should be fit to a theoretical model that combines both contributions in order to extract the area of the resonant CO transition, especially if the nonresonant contribution is changing during electrochemical oxidation.

In both IRAS and SFG spectroscopies, the signal intensity depends on both the surface coverage and an optical susceptibility. The susceptibility in SFG is the orientation-averaged molecular hyperpolarizability. Potential-dependent changes in intensity may result from changes in coverage and changes in orientation or hyperpolarizability [22]. In a bit of oversimplification, the SFG hyperpolarizability depends on both the infrared intensity (transition dipole moment) and the Raman intensity (polarizability), as well as the molecular orientation. On a metal surface, the intensity in the *ppp* polarization condition used here (infrared, visible and sum-frequency all polarized parallel to the plane of incidence) is sensitive to the molecular average tilt relative to the surface normal [26].

In order to use SFG as a quantitative probe of surface molecular coverage, therefore, one must properly acquire and analyze the SFG spectra

and be alert for the possibility that changes in SFG intensity are due to changing hyperpolarizability rather than surface coverage. Thus the SFG signal loss measured as a function of electrode potential may not accurately track the surface coverage loss for a number of reasons:

(1) The molecular-average tilt angle might change with electrode potential.
(2) The changing electric field may affect the CO dipole moment and polarizability.
(3) During electrooxidation, the CO lattice may transition through a variety of ordered and disordered phases resulting in different intermolecular interactions.
(4) During oxidation, anions may be coadsorbed, again resulting in different intermolecular interactions.
(5) The Pt surface may become chemically altered (e.g. oxidized) which could alter [27] the nonresonant contribution.

In this work, we have combined a broadband multiplex SFG apparatus [28,29] with a thin-layer electrochemical (TLE) cell apparatus, which results in several significant improvements over the prior art. In previous works using IRAS or SFG, the need to minimize infrared absorption in the aqueous electrolyte led to the use of cells where the electrode was pressed directly against the optical window. The electrolyte was then a thin film of uncertain depth, probably on the order of 1 or 2 μm. With such a thin film, the scan rate must be kept below a fraction of a mV/s to avoid a significant ohmic drop effect on the current–potential or current–time plots associated with surface redox processes. Due to the sensitivity of our SFG apparatus, we can tolerate a substantial amount of infrared attenuation due to absorption in the electrolyte layer so we are able to use a cell where thickness of the electrolyte film between the electrode and detector is controlled by a spacer. In the present work this spacer is 25 μm, which is compatible with a scan rate of 5 mV/s with minimal ohmic drop deformation. The SFG apparatus can obtain spectra in 200 ms or less, with a signal-to-noise >100:1 needed to extract the resonant amplitude A_v, the nonresonant amplitude A_{NR}, the CO peak frequency ω_v, the CO Lorentzian linewidth Γ_v, and the phase difference ϕ between the CO and nonresonant signals. The high potential scan and spectral acquisition rates minimize the possibilities for chemical contamination. They also enable a variety of future applications involving measurements of chemical kinetics on millisecond time scales commensurate with rates of surface poisoning in fuel cell electrocatalysis.

2. Vibrational sum-frequency generation spectroscopy (SFG)

In SFG, a simultaneous visible and vibrational infrared pulse are incident on the sample and a coherent sum-frequency signal is detected. The SFG signal exhibits characteristic features at frequencies of molecular vibrational resonances similar to the vibrational fingerprints of conventional FTIR spectroscopy [30]. SFG is a powerful method for investigating the vibrational transitions of molecules at interfaces, since it helps solve the two biggest problems of interfacial molecular spectroscopy, sensitivity and selectivity. Although the number density of interfacial molecules is low, the combination of intense femtosecond pulses (typically 10 GW/cm^2), coherence (the signal is emitted and collected as a coherent beam), and the very high sensitivity of CCD detectors to the visible sum-frequency photons generates adequate signals from many interfacial species. SFG is a three-photon process, so (in the dipole approximation) there is no SFG signal generated in centrosymmetric media [24]. At the interface between two such media (say oil and water) molecules in the bulk are ignored and molecules at the interface are selectively probed. In our electrochemistry experiments, an opaque electrode is covered by a dielectric aqueous electrolyte. In this configuration, SFG ignores molecules in the electrolyte and selectively probes adsorbed molecules at the symmetry-breaking electrode surface. Attenuation of the infrared beam by the electrolyte is less of a concern in SFG than in IRAS, since the infrared beam need not double-pass the electrolyte in SFG.

SFG is a well-known spectroscopic technique and the subject of several reviews [30–33], which

has so far been applied to electrochemical interfaces in a few cases [1–4,34,35]. We have developed an extremely powerful broadband multiplex SFG spectrometer [29]. The infrared pulse is a broadband femtosecond pulse spanning an $\sim$250 cm^{-1} region, the narrowband visible (here 804 nm) pulse is a picosecond pulse with 4 cm^{-1} FWHM, and the SFG signal is detected with a spectrograph and multichannel CCD detector. The center frequency of the infrared pulse and its spectral width determines which portion of the infrared region is being probed. The width of the visible pulse determines the spectroscopic resolution [28]. Our 4 cm^{-1} spectral resolution allows for accurate lineshape measurements of the $\sim$11 cm^{-1} FWHM CO stretching transition. With multiplex SFG it is possible to obtain the entire SFG spectrum in a selected region, e.g. the CO stretching region, with high signal-to-noise ratio in a short time interval. Here streams of spectra with signal-to-noise ratios >100:1 were obtained every 200 ms. This can be compared to conventional narrow-band SFG used in previous electrochemical measurements, where spectra with signal-to-noise ratios of $\sim$20:1 were obtained every 22 s [4] or spectra with signal-to-noise ratios of $\sim$100:1 were obtained in 65 min [3].

The SFG spectrum is a combination of the resonant molecular transitions plus a nonresonant background from the metal electrode surface. There is also a contribution from the water: CaF_2 interface. The water spectrum in the 1925–2175 cm^{-1} range is broad and weak, so this contribution is almost negligible. In analyzing our spectra, this is a minor correction to the nonresonant background that is removed during the fitting procedure. Ordinarily the molecular transitions are taken as Lorentzian lineshape functions and the nonresonant contribution is flat over the region of interest [25]. When the visible pulse is much narrower than the Lorentzian FWHM and the infrared pulse spectrum is flat across the region of interest,

$$\begin{aligned} I_{\mathrm{SFG}}(\omega) &\propto |\chi^{\langle 2\rangle}_{\mathrm{res}}(\omega) + \chi^{\langle 2\rangle}_{\mathrm{NR}}|^2 \\ &= ||\chi^{\langle 2\rangle}_{\mathrm{res}}(\omega)| \exp(\mathrm{i}\phi_{\mathrm{res}}(\omega)) \\ &\quad + |\chi^{\langle 2\rangle}_{\mathrm{NR}}| \exp(\mathrm{i}\phi_{\mathrm{NR}})|^2 \end{aligned} \tag{1}$$

where χ denotes a second-order susceptibility. In SFG experiments, only the phase difference, $\phi = |\phi_{\mathrm{res}} - \phi_{\mathrm{NR}}|$ is measured directly, as shown in Eqs. (3) and (4) below. The resonant susceptibility is approximated as,

$$\chi^{\langle 2\rangle}_{\mathrm{res}}(\omega) = \sum_v \frac{NA_v}{\omega - \omega_v + \mathrm{i}\Gamma_v/2} \tag{2}$$

N is the molecular number density, and the spectrum is a sum of Lorentzian lineshapes characterized by amplitudes A_v, central frequencies ω_v and linewidths (FWHM) Γ_v. The amplitude factors are proportional to the product of the orientation-averaged transition dipole moment and polarizability.

Our *ppp* polarized spectra are dominated by a single molecular transition due to top-site CO [2], and in this case, Eq. (1) becomes

$$\begin{aligned} I_{\mathrm{SFG}}(\omega) \propto{}& |\chi^{\langle 2\rangle}_{\mathrm{res}}(\omega)|^2 + |\chi^{\langle 2\rangle}_{\mathrm{NR}}|^2 \\ &+ 2|\chi^{\langle 2\rangle}_{\mathrm{res}}(\omega)||\chi^{\langle 2\rangle}_{\mathrm{NR}}| \cos(\phi) \end{aligned} \tag{3}$$

Eq. (3) shows that if the $\chi_{\mathrm{res}} \gg \chi_{\mathrm{NR}}$, $I_{\mathrm{SFG}} \propto N^2$ and the resonant lineshape is approximately the square of the Lorentzian function. When $\chi_{\mathrm{NR}} \gg \chi_{\mathrm{res}}$, the resonant signal is heterodyne-detected against a local oscillator (the nonresonant background), the lineshape is approximately Lorentzian atop a flat plateau, and $I_{\mathrm{SFG}} \propto N$. When both terms contribute significantly, the lineshape is not Lorentzian and I_{SFG} is proportional to N raised to a power between 1 and 2. In order to extract CO molecular parameters, SFG spectra were fit to the following expression,

$$\begin{aligned} I_{\mathrm{SFG}}(\omega) \propto{}& \left[\frac{(\omega - \Omega)^2}{2\delta^2}\right] \\ &\times \left|A_{\mathrm{NR}} \exp(-\mathrm{i}\phi) + \frac{NA_v}{\omega - \omega_v + \mathrm{i}\Gamma_v}\right|^2 \end{aligned} \tag{4}$$

The first factor in Eq. (4) accounts for the broadband infrared pulse spectrum, which is fit by a Gaussian function centered at frequency Ω ($\Omega \approx 2070$ cm^{-1}) with width δ ($\delta \approx 100$ cm^{-1}). Before every run, the Gaussian parameters are determined and held fixed throughout the fitting procedure. A series of SFG spectra are then fit

by varying the parameters A_{NR}, ϕ, NA_v, ω_v and Γ_v. As shown in Fig. 3E–G and Fig. 5E–G, Eq. (4) provides an excellent fit to all SFG spectra.

3. Experimental

The TLE SFG electrochemical cell depicted in Fig. 1 was made of Kel-F and glass with a 60° CaF_2 prism (Wilmad Glass) as the input window [36,37]. The working electrode was a 5 mm diameter Pt disk embedded in a Teflon holder, so that only one polished surface contacted the electrolyte. A 25 μm thick Teflon spacer was placed between the electrode and the CaF_2 prism. The Teflon holder was used as a plunger to compress the spacer between the electrode and the prism to create a uniform electrolyte layer of known thickness. Electrode potentials were measured against a commercial Ag/AgCl electrode (BAS) that was connected to the cell via electrolyte-filled tubing. Chemicals used were sulfuric and perchloric acid (GFS, double distilled from Vycor), CO (Matheson, research purity) and Millipore water. Cyclic voltammetry measurements used a PAR 263A potentiostat interfaced with a personal computer via Corrware software. Measurements were made using both CO-saturated electrolyte and CO-free electrolyte.

For SFG spectroscopy, 804 nm pulses of ~2 mJ energy and 200 fs duration were generated at 1 kHz using a femtosecond amplified Ti:Sapphire laser described elsewhere [29]. About 1.8 mJ of the pulse

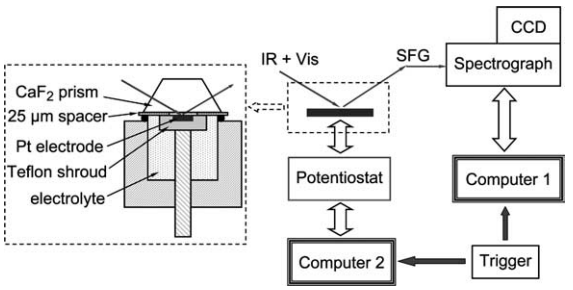

Fig. 1. Experimental schematic. (left) Electrochemical cell with a 25 μm Teflon spacer that provides an electrolyte layer of known and controlled thickness. (right) A CCD detector acquires broadband multiplex SFG spectra. The potentiostat and the CCD are synchronized with a common trigger.

was used to pump an optical parametric amplifier (Light Conversion, TOPAS DFG) that generates femtosecond ~200 cm^{-1} FWHM infrared pulses centered at 4.8 μm. The remaining 804 nm (visible) beam is spectrally filtered to 4 cm^{-1} FWHM. The p-polarized infrared and visible beams are combined with a dichroic mirror, and owing to the CaF_2 prism they are incident on the electrode surface at an angle of 60°. The visible pulse energy is 1 μJ, the duration is 4 ps and the $1/e^2$ beam radius is $r_0 = 100$ μm. The IR pulse energy is 10 μJ, the duration is 200 fs and $r_0 = 125$ μm. With a near-Gaussian beam profile, the fluence is greatest at the center of the pulse. The 60° incidence doubles the beam area on the prism and electrode surfaces. Accounting for both effects, the fluence at the center of each pulse is given by J_c = (pulse energy)/(πr_0^2), and J_c = 20 mJ/cm^2 for the IR and J_c = 3 mJ/cm^2 for the visible. For water, the absorption coefficient in the visible is negligible, and in the IR it is $\alpha = 400$ cm^{-1} [38]. With a 25 μm path length at 60°, the IR is attenuated by a factor of $\exp(-\alpha L) = \exp(-2)$ when it reaches the electrode surface, so the IR fluence at the electrode $J_c = 2.7$ mJ/cm^2. A short pass filter (Omega Optical) cuts out the visible light at 804 nm and transmits the SFG signal centered near 686 nm. The SFG signal is detected with a 0.25 m Chromex spectrograph and an Andor CCD detector. The SFG spectra were fit to Eq. (4) using SigmaPlot software.

The cyclic voltammetric and SFG measurements were carried out simultaneously. The CCD detector and the potentiostat were synchronized in an open-loop configuration by starting the experiment with a common trigger. Careful measurements were used to show that both devices remained well synchronized throughout the duration of each SFG-voltammetry run. The potentiostat scanned the electrode potential at 5 mV/s while the CCD was read out at 5 spectra/s.

Measurements were made with the electrochemical apparatus at room temperature, $T = 23 \pm 2$ °C. We have done calculations to estimate the laser-induced temperature increase ΔT. The calculations are done in two stages. First we calculate the single-pulse adiabatic temperature jump ΔT_a, and then include effects of thermal conduction.

In the electrolyte heated by the IR pulse, $\Delta T_a = J\alpha/\rho C$, where J is the fluence, $\alpha = 400\ \mathrm{cm}^{-1}$ [38] is the absorption coefficient and ρ and C the density and heat capacity. At the CaF_2 surface $\Delta T_a = 2$ K and at the electrode surface (the electrode reflects 98.5% of the IR) $\Delta T_a = 0.5$ K. To determine the steady-state temperature rise with an infinite series of 1 kHz pulses, we used a 1D thermal conduction calculation that allows the electrolyte in the gap to cool by thermal conduction into the CaF_2 prism and the Pt electrode (see Fig. 1). The calculation shows that both the CaF_2 and Pt surfaces return to ambient between each pulse, and the hottest region of electrolyte within the gap has a steady-state temperature rise of $\Delta T = 1.5$ K.

Understanding Pt electrode heating is more complicated. Only single-pulse effects are important since the Pt electrode cools back to ambient between laser shots. The laser pulse heats a skin layer ~5 nm thick. Even with fs heating there is time for considerable thermal conduction into Pt, so the fs IR pulse is more important than the ps visible pulse. To estimate the surface temperature in a way that accounts for thermal conduction we look at a related process, fs ablation. Experiment shows that a femtosecond 400 nm pulse at $J = 140\ \mathrm{mJ/cm^2}$ ablates the Pt surface [39]. Presumably such a pulse jumps the surface temperature to near the boiling point of ~4000 K. Pt absorption for IR is about 2.5 times less than at 400 nm. Our IR fluence is $J = 2.7\ \mathrm{mJ/cm^2}$. Thus our IR pulse would be expected to jump the Pt surface temperature by $\Delta T \approx 30$ K. The SFG signal is emitted by CO during an ~1 ps free-induction decay initiated by the IR pulse, so the CO spectrum actually depends on how much the hot electrode surface heats the CO vibrations during this period. The time constant for a laser pulse to heat CO has been estimated at ~1.5 ps [40]. Thus the SFG spectrum is generated while CO is somewhat colder than the Pt surface. Based on these time constants, we estimate $\Delta T < 10$ K for CO on Pt.

4. Results

A series of SFG spectra of CO adsorbed on Pt electrode in CO-free 0.1 M H_2SO_4 electrolyte is shown in Fig. 2. In spectra with higher CO coverage, the ratio of RMS noise to the CO peak amplitude exceeds 100:1. The asymmetrical shape of the SFG peak results from the previously mentioned interference between a resonant Lorentzian CO contribution and the Pt nonresonant background. When oxidation commences the SFG signal drops precipitously.

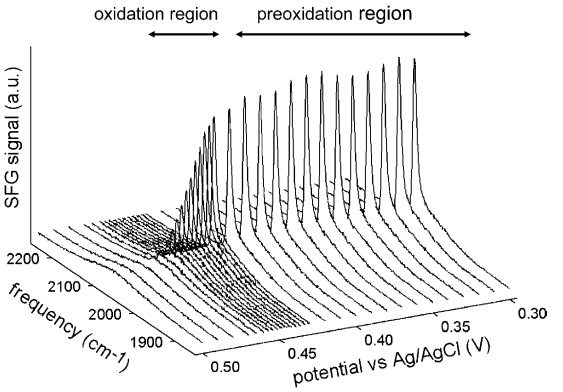

Fig. 2. A series of SFG spectra in the CO stretch region with CO-free 0.1 M H_2SO_4 electrolyte. The electrode potential is swept at a rate of 5 mV/s, and SFG spectra are obtained every 200 ms. Although spectra were obtained at 1 mV intervals, to avoid congestion in this plot averaged spectra are displayed at 10 mV intervals in the preoxidation region ($V < 0.43$ V) and at 3.3 mV intervals in the oxidation region ($V > 0.43$ V).

Fig. 3 shows electrochemical-SFG results obtained simultaneously in a cell with CO-free electrolyte. Fig. 3A shows the CO stripping 2-cycle voltammetry. The hydrogen peaks are completely suppressed and the CO adlayer is stable from the hydrogen evolution potential to about 0.4 V. The voltammetric CO oxidation peak begins at ~0.42 V and ends at ~0.51 V. In the second scan (dashed lines), there is no oxidation current and the hydrogen adsorption–desorption peaks are fully recovered.

Some typical SFG spectra and fits from Eq. (4) are shown at right (Fig. 3E–G). The fits are excellent even at lower signal levels, which verifies that the CO lineshape is Lorentzian. Fig. 3B shows the resonant and nonresonant amplitudes and the phase angle ϕ as a function of electrode potential. The resonant amplitude NA_v rises slightly in the preoxidation region. Once oxidation begins the

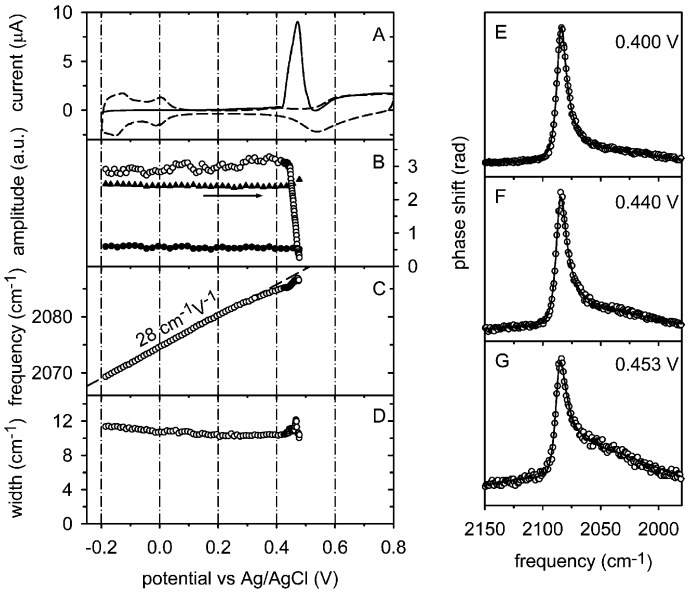

Fig. 3. Simultaneous SFG and electrochemical measurements with CO free 0.1 M H_2SO_4 electrolyte. (A) CO stripping voltammogram. (B) Resonant SFG amplitude (open circles), nonresonant SFG amplitude (filled circles) and phase difference (triangles). (C) CO stretch frequency shift. In the preoxidation region the frequency shift is fit by a line with the indicated slope. At the onset of oxidation the shift shows a dip and recovery, relative to this line. (D) Vibrational linewidth. (E–G) SFG spectra (open circles) at the indicated potential along with theoretical fits (solid curves) from Eq. (4).

resonant signal drops sharply. The nonresonant amplitude and phase angle remain constant throughout the electrode potential scan.

The CO stretching frequency in Fig. 3C increases linearly until ~0.30 V. The best linear fit yields a Stark tuning rate $d\omega_{CO}/dV = 28\ cm^{-1}/V$. A dashed line with this slope is drawn in Fig. 3C, showing that the slope is not constant above ~0.3 V. Compared to the (dashed) line of constant slope, the resonant frequency evidences a small dip (~1 cm^{-1}) and then a recovery. The Stark tuning rate is in good agreement with previous reports [3,4,8,9,19,41], and the dip and recovery is qualitatively but not quantitatively similar to what has been seen with infrared and SFG spectroscopies previously [2,4,42]. Fig. 3D shows that the CO peak width (FWHM) decreases slightly until CO oxidation begins. Then there is an increase and decrease in the FWHM that tracks the oxidation current.

Fig. 4 compares the resonant CO amplitude NA_v to the oxidation charge in the CO stripping region. The charge is obtained by direct numerical integration of the current in Fig. 3A. We emphasize that the voltammogram and the SFG spectra were obtained simultaneously in an optical TLE cell. Fig. 4 shows a high degree of coincidence between the CO amplitude and the charge. The amplitude and current are identical until about

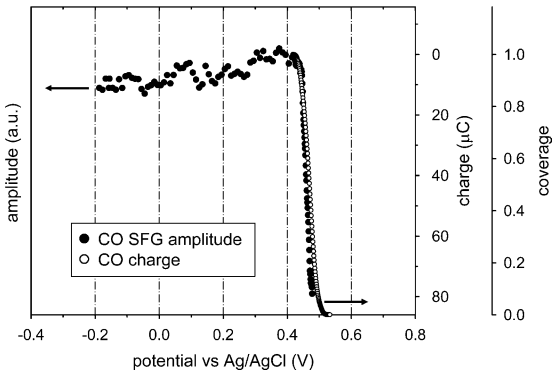

Fig. 4. Comparison (with CO-free electrolyte) of the SFG amplitude of the CO stretch (filled circles) with the charge (open circles). The charge is computed by numerical integration of the current shown in Fig. 3A.

the halfway point of the CO stripping process, where the amplitude seems to fall a bit faster than the current. These data are indicative of a precise correspondence between the current and SFG amplitude. Whatever small difference exists between the amplitude and charge data in the latter part of CO stripping may well result from experimental error, since the SFG signal-to-noise ratio decreases as CO is stripped from the Pt surface.

Fig. 5 shows results with a CO-saturated 0.1 M H_2SO_4 electrolyte. The voltammogram is shown in Fig. 5A. The current from the oxidation of both surface and solution CO are superimposed [43–45]. Solution CO oxidation starts as low as ~0.12 V, while the oxidation of surface CO begins at ~0.43 V and completes at ~0.52 V. Hydrogen peaks are completely suppressed upon the first scan, while on the second scan (dashed lines), only a minimal CO oxidation current was observed. The hydrogen peaks were recovered in the second scan, implying that most of the solution CO molecules were oxidized during the first potential cycle. This indicates the voltammetric cycle was completed faster than CO could diffuse from the bulk electrolyte to replenish the thin layer of the TLE cell.

Some representative SFG spectra along with their fits to Eq. (4) are shown in Fig. 5E–G. As in Fig. 3, the fits to a Lorentzian lineshape are excellent. Comparison of Figs. 3 and 5 highlights notable differences between CO-free and CO-saturated electrolytes. With CO-saturated electrolyte, the phase angle ϕ is no longer constant in the oxidation region. The phase angle drops suddenly when oxidation occurs and at the same time the nonresonant amplitude shows a very slight drop. The Stark tuning and linewidth behavior are qualitatively similar in both systems, but the dip and linewidth increase are greater with CO-saturated electrolyte. The Stark tuning rate $d\omega_{CO}/dV$ is the same within experimental error in both systems. However with the CO-saturated electrolyte, the CO frequency (in the preoxidation linear Stark region) is everywhere blueshifted by ~3 cm^{-1} compared to CO-free electrolyte. However at the dip minimum both CO-saturated and CO-free systems evidence the same frequency, $\omega_v = 2085\ cm^{-1}$. Consequently the dip is ~5 cm^{-1} deep compared

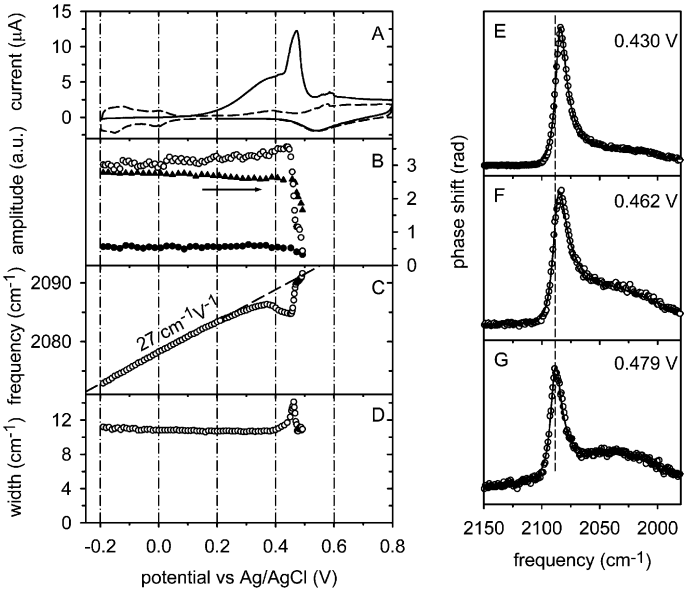

Fig. 5. Simultaneous SFG and electrochemical measurements with CO-saturated 0.1 M H_2SO_4 electrolyte. (A) CO stripping voltammogram. (B) Resonant SFG amplitude (open circles), nonresonant SFG amplitude (filled circles) and phase difference (triangles). (C) CO stretch frequency shift. (D) Vibrational linewidth. (E–G) SFG spectra (open circles) at the indicated potential along with theoretical fits (solid curves) from Eq. (4).

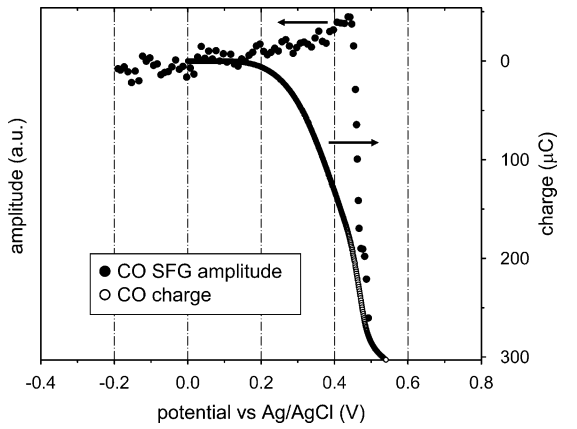

Fig. 6. Comparison (with CO-saturated electrolyte) of the SFG amplitude of the CO stretch (filled circles) with the charge (open circles). The charge is computed by numerical integration of the current shown in Fig. 5A.

to $\sim$1 cm^{-1} with CO-free electrolyte. The linewidth increase in the oxidation region with CO-saturated electrolyte is about double what is seen with CO-free electrolyte.

Fig. 6 compares the accumulated charge and the CO resonant amplitude with CO-saturated electrolyte. In contrast to Fig. 4, the SFG signal does not correspond exactly to the charge. The charge builds up to a considerable extent before the SFG signal starts to drop at $\sim$0.44 V. With the CO-saturated electrolyte, the two techniques measure different things. The current and charge are sensitive to the total number of CO equivalents oxidized in the electrolyte and on the Pt surface, whereas the SFG signal is sensitive to the CO stripping process, which reduces the CO surface coverage.

5. Discussion

Our SFG spectra were obtained with broadband multiplex spectroscopy, resulting in far higher signal-to-noise ratios than has been possible in previous work. We were also able to use a potential scan rate far greater than has been previously possible, which minimizes the possibilities for erroneous electrochemistry. We have been able to perform a highly detailed analysis of the SFG lineshape. This analysis reveals some interesting phenomena.

In this section we discuss the correspondence between charge and SFG amplitude, which has previously been the subject of some controversy. In addition we will address issues that arise from our detailed analysis of the SFG lineshape. These are the SFG amplitude increase in the run up to oxidation seen in Figs. 3B and 5B, the SFG frequency shift behavior in the oxidation region, and the SFG linewidth in the oxidation region.

5.1. SFG in the oxidation region

Fig. 4 shows that our measurements on polycrystalline Pt electrodes do not see the remarkable features reported in previous works on Pt electrodes. Baldelli et al. [2] reported that the SFG signal vanished $\sim$200 mV below the oxidation threshold, and Chou et al. [4] reported that the SFG signal intensity vanished immediately after the oxidation current reached its maximum. Instead Fig. 4 shows the SFG intensity perfectly tracks the oxidation current. Chou et al. [4] also reported that the SFG intensity approximately doubled in the run up to oxidation, whereas we see at most a 10% signal increase.

Our spectra with CO-free electrolyte demonstrate a remarkable consistency. In particular the nonresonant background signal has been completely characterized for the first time. We have shown that with CO-free electrolyte the nonresonant amplitude and phase angle remain constant throughout the oxidation process (Fig. 3B), but with a CO saturated electrolyte the phase angle drops significantly in the oxidation region. The different phase angle is an indication that oxidation with CO saturation results in somewhat different electrode surface properties. An alternative explanation is that the optical properties of the electrolyte are slightly different in the two cases.

As demonstrated in Fig. 4, we have unambiguously shown an essentially exact relationship between the charge and the SFG resonant amplitude with the CO-free electrolyte. As a result of prior radioactive labeling studies, a precise correspondence between the charge and the surface coverage has also been demonstrated [45]. Thus we

have shown that electrochemical-SFG is a *quantitative analytical technique*, inasmuch as with the model system of CO on Pt with a CO-free electrolyte, the SFG resonant amplitude is directly proportional to a high degree of accuracy to the surface coverage. The slight deviation in Fig. 4 between the charge and SFG amplitude near the end of the oxidation process is at present attributed to experimental error. It would be very interesting if further measurements established this slight deviation to be real. It is not outside the realm of possibility that the SFG signal amplitude might prove to be a *more accurate* measurement of surface coverage than the oxidation current. In fact that is exactly the case with CO-saturated electrolyte, where the current is sensitive to oxidation processes involving CO both in the electrolyte and on the surface, whereas SFG is sensitive solely to the surface coverage.

5.2. SFG amplitude in the preoxidation region

Figs. 3B and 5B show an ~10% increase in the resonant SFG amplitude with increasing electric field in the preoxidation region. There are two reasons the SFG amplitude could increase at constant surface coverage: better orientational ordering of the CO molecules or an increase in the molecular hyperpolarizability.

The SFG signal intensity in *ppp* polarization is proportional to $\langle\cos^2\theta\rangle$ where θ is the angle between the CO bond axis and the surface normal, and brackets indicate ensemble average [26]. The CO molecules adsorbed on a polycrystalline surface evidence a wide range of azimuthal angles and a smaller range of polar angles θ. The polar angle spread might result from surface topography, variations in chemical bonding or thermal disorder. The increase in SFG amplitude could then be attributed to electric-field-induced alignment of CO molecules to overall more upright configurations. This interpretation is supported by the linewidth narrowing, which is also indicative of greater molecular order.

The alternative explanation, a field-induced increase in molecular hyperpolarizability, seems less likely. As the field increases, the resonant frequency ω_v blueshifts. This blueshift is caused by a reduction in the back-donation of electrons from the Pt surface to the CO π^* antibonding orbitals. With a reduction in backbonding, both the CO dipole moment and the polarizability would be expected to decrease, which is the wrong direction to explain the SFG signal.

5.3. CO frequency shift and dip

The CO frequency has a linear shift with electrode potential with a slope of $\sim 27\ \mathrm{cm}^{-1}\ \mathrm{V}^{-1}$ until the onset of oxidation, when a dip and recovery are observed. The frequency $\omega_v = 2085\ \mathrm{cm}^{-1}$ at the bottom of the dip is identical with both CO-saturated and CO-free electrolyte, but owing to an overall blueshift in the CO-saturated frequency, the dip is about five times deeper with CO-saturated electrolyte. The bottom of the dip is at a potential slightly below the peak of the oxidation current.

Weaver and coworkers [9,23] have shown that the CO frequency at fixed potential undergoes a redshift with decreased CO coverage. The mechanism of this redshift is evidently related to an increase in the average spacing between CO molecules, that reduces the intermolecular interactions that are primarily a result of dipole–dipole interactions [9,23,46]. Although this simple explanation [4] provides a good starting point, it is not really sufficient to explain the data in Figs. 3C and 5C. In particular it does not explain the asymmetric shape (the dip is gradual and the recovery is abrupt), the deeper dip with CO-saturated electrolyte, and why the dip recovers when oxidation is almost complete. We will now address these issues to the extent possible with available data, based on the premise that the dip results primarily from changing interactions among CO molecules in the adlayer.

CO oxidation occurs via the Langmuir–Hinshelwood mechanism [47,48],

$$\mathrm{Pt{-}CO} + \mathrm{Pt{-}H_2O} \rightarrow \mathrm{CO_2} + 2\mathrm{H^+} + 2\mathrm{e^-} + 2\mathrm{Pt^*}$$

which produces free $\mathrm{Pt^*}$ sites that reduce the density of the CO adlayer. However this mechanism provides no insight into the spatial distribution of surface CO and the other adsorbed species (anions, water, oxygen, etc.) during the stripping pro-

cess. The microscopic details of this spatial arrangement determine the intermolecular interactions. When a vacancy is created in a dense ordered adlayer, the adlayer becomes disordered. Then, broadly speaking, four interrelated outcomes are possible. (1) The vacancy remains and the adlayer stays disordered. (2) The vacancy is filled by some species from the electrolyte, and the adlayer remains disordered. (3) CO diffusion on the surface fills in the vacancy, resulting in an equally dense adlayer of reduced total area. (4) CO diffusion causes the adlayer to reconstruct into new ordered phases having lower density and the same area. There is experimental evidence that all four possibilities occur to some extent. In particular, on Pt(1 1 1) during the first few percent of CO oxidation the CO adlattice remains in the Pt(1 1 1)(2×2) structure. With further oxidation the adlattice reconstructs to a less dense Pt(1 1 1) $(\sqrt{19}\times\sqrt{19})$ structure [49,50].

In comparing the CO-free and CO-saturated systems, in the preoxidation region, (e.g. 0.3 V) the CO frequency with saturated electrolyte is blueshifted $+2\ \mathrm{cm}^{-1}$. At the bottom of the dip ($\sim$0.46 V) the CO frequencies are identical. At the end of the oxidation process ($\sim$0.5 V) the CO frequency with saturated electrolyte is blueshifted $+4\ \mathrm{cm}^{-1}$. The blueshift in the preoxidation region clearly is the result of the higher surface coverage with a CO-saturated electrolyte. The other features are harder to explain with the available data. Although the frequency is identical in both cases at the bottom of the dip, it is unreasonable to conclude that the CO-free and CO-saturated systems are temporarily in the same state. The two systems start from different states and end up in different states, as judged by the frequency shift. This is indicative of the presence of offsetting effects, for instance a combination of differing CO and adsorbed anion structures. It is clear that the SFG peak shift provides information about the microscopic structure of the adlayer, but due to the coexistence of multiple species, the CO frequency by itself is not sufficient to extract all the information needed. Further experiments will be necessary, especially experiments where the CO concentration is varied at constant electrode potential and where the electrolyte is varied.

5.4. CO linewidth

Our fitting results indicate that the CO lineshape data are fit very well by Lorentzian functions. As the potential increases in the preoxidation region, the linewidth Γ decreases slightly. As CO oxidation begins; Γ first increases and then decreases. The maximum in Γ is near the peak oxidation current. The actual increase in Γ is small; the $\sim$11 cm^{-1} line broadens by either 2 or 3 cm^{-1} with CO-free and CO-saturated electrolytes.

Generally Lorentzian lineshapes of the type observed here are associated with homogeneous broadening. However since electrochemical oxidation of CO creates disorder in the adlayer, it seems natural to associate the linewidth increases with inhomogeneous broadening. The theory of vibrational lineshapes with both homogeneous and inhomogeneous processes is well developed [22 51]. Three parameters, T_2, Δ and τ, interact in a complicated way to determine the vibrational lineshape and linewidth Γ. The homogeneous width is characterized by the time constant for vibrational dephasing, T_2. The parameter Δ is the variance of the distribution of CO site energies. The energy of a site might fluctuate with time, and τ is the time constant for fluctuations in site energies. Together Δ and τ characterize the inhomogeneous broadening.

The variance Δ in CO site energies arises primarily from adlattice disorder, which results in a distribution of intermolecular interactions. The most important intermolecular interaction is the dipole–dipole coupling between nearby CO molecules. There are additional contributions from the disordered lattice of adsorbed anions and the local electrolyte structure. The time constant τ results from CO surface diffusion, CO and anion exchange between surface and electrolyte, and dynamical evolution of the local electrolyte structure.

Prior to oxidation, Δ is small, since CO is present in an ordered lattice, excepting defects and grain boundaries. CO stripping will first cause Δ to increase and then to decrease. The initial increase is caused by the generation of vacant CO sites. The decrease occurs at lower coverage when CO molecules are mostly isolated and see little

variance in intermolecular interactions. The details of the dynamical stripping process that includes defect formation and surface reconstruction must be very complicated and are at present poorly understood. A simple model is to view the surface as a disordered binary-mixed crystal in two dimensions, consisting of CO molecules and defects. In studies of the vibrational linewidths of binary-mixed molecular crystals [52,53], the linewidth is usually a minimum for the pure crystal and a maximum for the 50:50 mixed crystal. Thus it seems reasonable that the parameter Δ would be a maximum when about one-half of the CO has been stripped, at the peak of the oxidation current.

The parameter T_2 has two distinct contributions, characterized by time constants T_1 and T_2^*. T_1 is the lifetime of the excited ($v = 1$) CO vibration on the surface and T_2^* is a time constant for processes that interrupt the phase of the CO oscillator (pure dephasing). The vibrational lifetime T_1 of CO on Pt(1 1 1) results from energy transfer from CO vibrations to conduction electrons via nonadiabatic coupling [54,55]. This lifetime has been measured in vacuum [56,57], and also in aqueous electrolyte [58] and in liquid acetonitrile [59]. T_1 is in the 1.5–2.0 ps range, and only weakly dependent on electrode potential [58,59]. The linewidth corresponding to the vibrational lifetime, $\Gamma = 5.3$–$7\ \mathrm{cm}^{-1}$, is less than the observed $\Gamma = 11$–$14\ \mathrm{cm}^{-1}$, so pure dephasing appears to be dominant. Pure dephasing results from thermal fluctuations of the Pt surface, which randomly excite the Pt–CO adbond. Energy exchange between the lower frequency adbond and the CO stretch rapidly modulates the CO stretch frequency [60]. Pure dephasing might also result from fluctuating interactions between CO and electrolyte.

Based on this discussion, we attribute the small linewidth decrease in the preoxidation region to a small increase in the ordering of the CO adlattice. Increasing the electric field makes CO stand more upright, decreasing orientational disorder. The electric field increase can also increase the ordering of ions in the local electrolyte. Changes in Γ during CO oxidation reflect increases and decreases in the adlayer ordering during the CO stripping process. The greater increase in Γ with CO saturated electrolyte may be related to the increased likelihood of surface/solution CO exchange, as reported by Chorkendorff and coworkers [61], and recently confirmed on rough surfaces by McGovern et al. [45].

An interesting problem is why the data are fitted well by Lorentzian lineshapes. The most likely possibility is that disorder effects are only a small part of the lineshape that is dominated by pure dephasing. In this case the lineshape would be a Voigt function, a convolution of Lorentzian and Gaussian functions, but the overall Gaussian contribution is small and hard to detect. The other possibility relates to the parameter τ. When there is relatively rapid exchange between different environments, disorder adds a motionally-narrowed contribution to the lineshape of width $\Delta^2\tau$ [62] which gives a lineshape almost indistinguishable from Lorentzian. For motional narrowing to be of importance with $11\ \mathrm{cm}^{-1}$ linewidths, τ would have to be on the order of picoseconds. CO diffusion and CO-electrolyte exchange are too slow, but dynamic rearrangements in the local electrolyte might have this effect. Unfortunately spectral lineshape analysis is a tool with limited ability to sort out these complicated broadening issues, which suggests the need for more sophisticated vibrational echo experiments [63] in the future.

5.5. Summary and conclusions

Our advanced SFG-electrochemical apparatus permits rapid, accurate and simultaneous acquisition of voltammetric and spectroscopic data. Although SFG lineshapes resulting from coherent interactions are somewhat more complicated than ordinary linear IRAS, by obtaining high signal-to-noise spectra and fitting the lineshape to a theoretical model, we can accurately extract the resonant amplitude (proportional to surface coverage), resonant frequency and resonant linewidth, as well as the nonresonant amplitude and phase difference.

When we perform this analysis with the simpler CO-free electrolyte system, in contrast to previous works we obtain a remarkable agreement between the accumulated oxidation current (total charge) and the SFG amplitude, which clearly demonstrates the power of SFG as a quantitative tool for measuring surface coverage. We also show that as the electrode potential is changed, the nonreso-

nant amplitude and phase from the Pt surface remains essentially constant, and the resonant frequency undergoes a Stark shift at a rate of $28\ cm^{-1}\ V^{-1}$.

By comparing CO-free and CO-saturated electrolytes, we observe some interesting effects. At the onset of oxidation, there is a dip and recovery of the frequency, and the resonant linewidth reaches a maximum at the point of maximum current. With the CO-saturated electrolyte, these dip and linebroadening effects are larger. During the oxidation process, the phase shift of nonresonant signal (relative to the resonant signal) drops significantly in a way not seen with CO-free electrolyte.

These interesting features provide new insights into the microscopic dynamics of CO on the Pt surface. The frequency dip and recovery can be interpreted in terms of changing intermolecular interactions between CO molecules in the adlayer, and these observables are expected to be sensitive to the adsorption of anions, the oxidation of Pt sites, and the ordering and density of the CO adlayer. The linebroadening can be interpreted in terms of motional narrowing dynamics, where an inhomogeneous distribution of site energies resulting from disorder created by CO oxidation is modulated by fast motions of CO within the adlayer and between the adlayer and electrolyte. These effects are new and interesting, but further interpretation will require more detailed experimental investigations.

The use of SFG to probe electrochemical phenomena thus provides new insights in two distinctly different and interesting time and length domains. Changes in SFG amplitude on the millisecond time scale can be directly related to the total surface coverage. Changes in resonant frequency not associated with the Stark shift can be related to microscopic variations in the surface coverage and order. Changes in the resonant linewidth can be related to microscopic surface disorder and its interactions with motions of the CO molecules.

Acknowledgement

This work is supported by the US Department of Energy, Division of Materials Sciences under award no. DEFG02-91ER45439, through the Frederick Seitz Materials Research Laboratory at the University of Illinois at Urbana-Champaign, and by the National Science Foundation under grant NSF CHE03-4999. Additional support was provided by the Army Research Office (DDD grant is DAAD19-03-1-0169).

References

[1] P. Guyot-Sionnest, A. Tadjeddine, Chem. Phys. Lett. 172 (1990) 341.
[2] S. Baldelli, N. Markovic, P. Ross, Y.R. Shen, G. Somorjai, J. Phys. Chem. B 103 (1999) 8920.
[3] F. Dederichs, K.A. Friedrich, W. Daum, J. Phys. Chem. B 104 (2000) 6626.
[4] K.C. Chou, N.M. Markovic, J. Kim, P.N. Ross, G.A. Somorjai, J. Phys. Chem. B 107 (2003) 1840.
[5] J.W. Russell, M. Severson, K. Scanlon, J. Overend, A. Bewick, J. Phys. Chem. 87 (1983) 293.
[6] B. Beden, N. Collas, C. Lamy, J.M. Leger, V. Solis, Surf. Sci. 162 (1985) 789.
[7] K. Kunimatsu, H. Seki, W.G. Golden, J.G. Gordon, M.R. Philpott, Langmuir 2 (1986) 464.
[8] C. Korzeniewski, S. Pons, P.P. Schmidt, M.W. Severson, J. Chem. Phys. 85 (1986) 4153.
[9] D.S. Corrigan, M.J. Weaver, J. Electroanal. Chem. 241 (1988) 143.
[10] A. Czerwinski, Anal. Lett. 22 (1989) 1547.
[11] W.F. Lin, S.G. Sun, Z.Q. Tian, Z.W. Tian, Electrochim. Acta 38 (1993) 1107.
[12] P.J. Slezak, A. Wieckowski, J. Magn. Reson. Ser. A 102 (1993) 166.
[13] T. Iwasita, F.C. Nart, Prog. Surf. Sci. 55 (1997) 271.
[14] A.V. Petukhov, W. Akemann, K.A. Friedrich, U. Stimming, Surf. Sci. 404 (1998) 182.
[15] N.M. Markovic, P.N. Ross, Surf. Sci. Rep. 45 (2002) 121.
[16] M.T.M. Koper, N.P. Lebedeva, C.G.M. Hermse, Faraday Discuss 121 (2002) 301.
[17] F. Vidal, B. Busson, A. Tadjeddine, A. Peremans, J. Chem. Phys. 119 (2003) 12492.
[18] J.W. Russell, J. Overend, K. Scanlon, M. Severson, A. Bewick, J. Phys. Chem. 86 (1982) 3066.
[19] Z.Q. Tian, B. Ren, B.W. Mao, J. Phys. Chem. B 101 (1997) 1338.
[20] S.G. Sun, S.J. Hong, S.P. Chen, G.Q. Lu, H.P. Dai, X.Y. Xiao, Sci. China Ser. B 42 (1999) 261.
[21] A. Miki, S. Ye, M. Osawa, Chem. Commun. (2002) 1500.
[22] S. Mukamel, Principles of Nonlinear Optical Spectroscopy, Oxford University Press, New York, 1995.
[23] L.W.H. Leung, A. Wieckowski, M.J. Weaver, J. Phys. Chem. 92 (1988) 6985.
[24] Y.R. Shen, Nature 337 (1989) 519.
[25] C.D. Bain, J. Chem. Soc. Faraday Trans. 91 (1995) 1281.

[26] C. Hirose, N. Akamatsu, K. Domen, Appl. Spectrosc. 46 (1992) 1051.
[27] A. Le Rille, A. Tadjeddine, J. Electroanal. Chem. 467 (1999) 238.
[28] L.T. Richter, T.P. Petralli-Mallow, J.C. Stephenson, Opt. Lett. 23 (1998) 1594.
[29] J. Patterson, A.S. Lagutchev, W. Huang, D.D. Dlott, Phys. Rev. Lett. 94 (2005) 015501.
[30] Y.R. Shen, Surf. Sci. 300 (1994) 551.
[31] K.B. Eisenthal, Ann. Rev. Phys. Chem. 43 (1992) 627.
[32] G.L. Richmond, Chem. Rev. 102 (2002) 2693.
[33] Z. Chen, Y.R. Shen, G.A. Somorjai, Ann. Rev. Phys. Chem. 53 (2002) 437.
[34] K.C. Chou, J. Kim, S. Baldelli, G.A. Somorjai, J. Electroanal. Chem. 554 (2003) 253.
[35] S. Hoffer, S. Baldelli, K. Chou, P. Ross, G.A. Somorjai, J. Phys. Chem. B 106 (2002) 6473.
[36] F. Vidal, B. Busson, C. Six, O. Pluchery, A. Tadjeddine, Surf. Sci. 502 (2002) 485.
[37] M.E. Biggin, A.A. Gewirth, J. Electrochem. Soc. 148 (2001) C339.
[38] D.M. Wieliczka, S. Weng, M.R. Querry, Appl. Opt. 28 (1989) 1714.
[39] K. Venkatakrishnan, B. Tan, N.V. Sivakumar, Opt. Laser Technol. 34 (2002) 575.
[40] M. Bonn, D.N. Denzler, S. Funk, M. Wolf, Phys. Rev. B 61 (2000) 1101.
[41] K. Kunimatsu, W.G. Golden, H. Seki, M.R. Philpott, Langmuir 1 (1985) 245.
[42] V. Stamenkovic, K.C. Chou, G.A. Somorjai, P.N. Ross, N.M. Markovic, J. Phys. Chem. B 109 (2005) 678.
[43] J.A. Caram, C. Gutierrez, J. Electroanal. Chem. 346 (1993) 451.
[44] A. Wieckowski, M. Rubel, C. Gutierrez, J. Electroanal. Chem. 382 (1995) 97.
[45] M.S. McGovern, P. Waszczuk, A. Wieckowski, J. Electroanal. Chem., submitted for publication.
[46] P. Hollins, J. Pritchard, Prog. Surf. Sci. 19 (1985) 275.
[47] M.T.M. Koper, A.P.J. Jansen, R.A. Vansanten, J.J. Lukkien, P.A.J. Hilbers, J. Chem. Phys. 109 (1998) 6051.
[48] N.P. Lebedeva, M.T.M. Koper, J.M. Feliu, R.A. van Santen, J. Phys. Chem. B 106 (2002) 12938.
[49] N.M. Markovic, C.A. Lucas, A. Rodes, V. Stamenkovi, P.N. Ross, Surf. Sci. 499 (2002) L149.
[50] Y.V. Tolmachev, A. Menzel, A.V. Tkachuk, Y.S. Chu, H.D. You, Electrochem. Solid State Lett. 7 (2004) E23.
[51] M.D. Fayer, Ultrafast Infrared and Raman Spectroscopy, Marcel Dekker, Inc., New York, 2001.
[52] E.L. Chronister, D.D. Dlott, J. Chem. Phys. 79 (1983) 5286.
[53] F. Ho, W.-S. Tsay, J. Trout, S. Velsko, R.M. Hochstrasser, Chem. Phys. Lett. 97 (1983) 141.
[54] M. Morin, N.J. Levinos, A.L. Harris, J. Chem. Phys. 96 (1992) 3950.
[55] M. Head-Gordon, J.C. Tully, J. Chem. Phys. 96 (1992) 3939.
[56] J.D. Beckerle, M.P. Casassa, R.R. Cavanagh, E.J. Heilweil, J.C. Stephenson, Phys. Rev. Lett. 64 (1990) 2090.
[57] J.D. Beckerle, R.R. Cavanagh, M.P. Casassa, E.J. Heilweil, J.C. Stephenson, J. Chem. Phys. 95 (1991) 5403.
[58] A. Peremans, A. Tadjeddine, P. GuyotSionnest, Chem. Phys. Lett. 247 (1995) 243.
[59] M.E. Schmidt, P. Guyot-Sionnest, J. Chem. Phys. 104 (1996) 2438.
[60] C.B. Harris, R.M. Shelby, P.A. Cornelius, Phys. Rev. Lett. 38 (1977) 1415.
[61] J.C. Davies, R.M. Nielsen, L.B. Thomsen, I. Chorkendorff, A. Logadottir, Z. Lodziana, J.K. Norskov, W. Li, B. Hammer, S.R. Longwitz, et al., Fuel Cells 4 (2004) 309.
[62] R. Kubo, J. Phys. Soc. Jpn. 9 (1954) 888.
[63] K.D. Rector, M.D. Fayer, Int. Rev. Phys. Chem. 17 (1998) 261.